DIRECT AND LARGE-EDDY SIMULATIONS OF TURBULENT HEAT TRANSFER IN TAYLOR-COUETTE FLOWS WITH A STATIONARY GROOVED OUTER CYLINDER

Y. Amano*, **K. Takeda, Y. Kuwata, M. Kaneda, K. Suga**
Department of Mechanical Engineering
Osaka Metropolitan University
1-1, Gakuen-cho, Naka-ku, Sakai, Osaka 599-8531, Japan
*sg23896j@st.omu.ac.jp

ABSTRACT

To understand the grooved stator effects on torque and heat transfer performance of electric vehicle drive-motors, we have performed direct and large-eddy simulations of Taylor-Couette (TC) flows with an axially grooved stationary cylinder. The radius ratio of the present TC flow configuration is $\eta = 0.955$ and the Reynolds number Re is up to 21000 ($Re = 175, 300, 1050, 3500, 10500, 21000$). Cases TC and O48 are considered. Case TC is a usual grooveless TC flow with a stationary outer cylinder. Case O48 has a 48 grooved outer cylinder. Additionally, to compare grooved inner cylinder flows, Case I32 which has a rotating 32 grooved inner cylinder is considerd. The results show that the effects of grooves are evident for torque and heat transfer when the Taylor number Ta is greater than 10^8. The transition to the ultimate turbulent regime that corresponds to a fully turbulent flow appeares $10^7 < Ta < 10^8$ in Cases I32 and O48. In the grooved cases, the contribution of the Reynolds stress to torque is much larger than that in Case TC. The effect of the grooves on torque and heat transfer increases with Ta owing to the pressure drag and heat transfer from the grooves. At $Ta > 10^8$, streak structures appear and Case O48 shows that the streak structure extends over the entire region near inner wall. At $Ta \simeq 10^7$, the premultiplied energy spectra (PMS) has a peak at the wave length of the Taylor vortices, while at $Ta \simeq 10^8$, another peak appears at $\lambda_z^+ \simeq 100$, which coincides the spanwise streak spacing of a turbulent boundary layer. This trend is remarkable in Case O48 and related to the earlier transition to the ultimate turbulent regime.

INTRODUCTION

Since the TC flows, which are flows in concentric annuli with rotating cylinders, appear in many engineering devices such as gas turbines and chemical reactors, torque and heat transfer characteristics of the TC flows have been studied by many researchers (e.g. Grossmann *et al.*, 2016). Ostilla-Mónico *et al.* (2014*a*) reported that torque could be scaled by the Taylor number. The drive-motors used in electric vehicles (EVs) can be also modelled as concentric annuli consisting of a rotating inner cylinder (rotor) and a stationary outer cylinder (stator). The rotor and stator usually have groove-shaped roughness which significantly affects the torque and heat transfer performance. It is thus essential to understand the effects of grooves on torque and heat transfer characteristics for designing high performance EV motors. In this study, we consider grooved Taylor-Couette (GTC) flows as simplified flow configurations for the flows in the EV motors. Although many other studies focused on the characteristics of rib-roughened or grooved TC flows (Bouafia *et al.*, 1998; Zhu *et al.*, 2018), little is known about characteristics in the axially grooved TC flows. Therefore, we perform direct and large-eddy simulations (DNS and LES) of axially grooved TC turbulent flows by the lattice Boltzmann method (LBM) to understand the effects of the grooves on torque and heat transfer in EV motors.

Table 1. Computational conditions.

model	Re	Ta	Δ^+
DNS	$175-10500$	$3\times10^4-10^8$	$1.8-1.9$
LES	21000	5×10^8	$2.9-3.6$

NUMERICAL METHODS

In this study, we apply the D3Q27 multiple-relaxation time lattice Boltzmann method (MRT-LBM) (Suga *et al.*, 2015) and the D3Q19 reguralized single-relaxation time lattice Boltzmann method (SRT-LBM) (Suga *et al.*, 2017) for simulating the flow and thermal fields, respectively. Temperatures are treated as passive scalars without buoyancy effects. We apply the interpolated bounce-back scheme to the curved boundary walls in the Cartesian grid system. The presently applied sub-grid-scale (SGS) model is the shear-improved Smagorinsky model by Lévêque *et al.* (2007), where the SGS eddy viscosity ν_{SGS} is given as $\nu_{SGS} = (C_s\Delta)^2(|\bar{S}| - |\langle\bar{S}\rangle_t|)$, where $|\bar{S}|$ represents the strain rate, $|\langle\bar{S}\rangle_t|$ is the time-averaged strain rate, $C_s = 0.16$, and Δ is the grid spacing. The SGS thermal diffusivity α_{SGS} is given as $\alpha_{SGS} = \nu_{SGS}/Pr_{SGS}$, with the SGS turbulent Prandtl number $Pr_{SGS} = 0.9$.

FLOW GEOMETRY AND COMPUTATIONAL CONDITIONS

Fig.1 shows the computational domains and geometries. We consider the grooved Taylor-Couette (GTC) flows of Cases I32 and O48 which have 32 grooves on the rotor wall and 48 grooves on the stator wall, respectively. For reference, non-grooved TC flows are also simulated. To save the computational costs, we have considered one quarter of the cylinder for the computational domain. The axial domain length is

$L_z = 2.5d$ for $Re = 10500, 21000$ or $5.0d$ for $Re \le 3500$ with d being the gap between the rotor and stator. The rotor and stator radii in the present cases are $r_i = 21d$ and $r_o = 22d$, respectively, which yields the radius ratio of $\eta = r_i/r_o = 0.955$ for all cases. The periodic boundary conditions are used in the axial (z) and azimuthal (θ) directions, and a constant temperature difference between the inner cooled wall ($T = T_i$) and outer heated wall ($T = T_o$) is imposed. In all cases, the outer cylinder is stationary, and the inner cylinder rotates with an angular velocity ω_i. For Case I32, we apply the rotating coordinate system to simulate the rotor rotation without moving-boundaries, and the Coriolis force and centrifugal forces are added to the force term in the LBM. The Reynolds and Taylor numbers are defined as $Re = r_i\omega_i d/\nu$, $Ta = (1+\eta)^6 Re^2/(64\eta^4)$ respectively, where ν is the fluid kinematic viscosity. Table 1 shows the computational conditions of this study. We have performed DNS up to $Re = 10500$ ($Ta = 1.16\times10^8$) and LES at $Re = 21000$ ($Ta = 4.63\times10^8$). The grid resolution is defined as $\Delta^+ = \Delta u_{\tau,i}/\nu$, where $u_{\tau,i}$ is the friction velocity at the rotor wall. The structured regular grid system is applied to all cases and Δ^+ is designed to be always less than 2 for DNS. The total number of grid points occupied by the fluid phase for Case O48 at $Re = 21000$ is 1529514600. The Prandtl number is set to 0.71 assuming that the working fluid is air. Since the LBM is based on the Cartesian grid system, we transform the results to those in the cylindrical coordinates for the disccussion.

RESULTS AND DISCUSSION

Torque and heat transfer

The key response parameter of the TC system is G^ω which is the normalized torque τ by the laminar angular velocity flux $J^\omega_{\rm lam}$ (Grossmann *et al.*, 2016). It is defined as $G^\omega = \tau/(2\pi L_z\rho J^\omega_{\rm lam})$ where $J^\omega_{\rm lam} = 2\nu r_i^2 r_o^2\omega/(r_o^2 - r_i^2)$ for the stationary outer cylinder cases. Fig.2 (a) shows G^ω against Ta. At $Ta \le 10^7$, the effective scaling exponents of $G^\omega \sim Ta^\alpha$ for Cases GTCs (I32 and O48) are almost the same as that of Case TC. At $Ta \ge 10^8$, the effects of the grooves become evident, and G^ω for Cases GTCs deviate upward from the non-grooved TC flow results.

For the effective scaling exponent of $G^\omega - 1 \sim Ta^\alpha$ in TC flows, summarizing the literature, Grossmann *et al.* (2016) reported that $\alpha = 1/3$ was observed from $Ta \simeq 10^4$ to $Ta \simeq 3\times10^6$ after the onset of Taylor vortices and called the laminar regime. And the classical turbulent regime with $\alpha < 1/3$ occured up to $Ta \simeq 3\times10^8$. For $Ta > 3\times10^8$, not only the bulk region but also the boundary layer became turbulent and $1/3 < \alpha \le 1/2$ was observed, which was called the ultimate turbulent regime (Ostilla-Mónico *et al.*, 2014*b*). In the ultimate turbulent regime for TC flow, the scaling exponent reached $\alpha \simeq 0.38$ (Ostilla-Mónico *et al.*, 2014*a*).

Fig.3 shows the present $(G^\omega - 1)/Ta^{1/3}$ against Ta along with the results of Ostilla-Mónico *et al.* (2014*a*) and Zhu *et al.* (2018). In the present cases, in the range of $Ta \simeq 10^6 - 10^7$, the scaling exponent α asymptotically approaches $1/3$ since $(G^\omega - 1)/Ta^{1/3}$ approaches constant values. In Cases GTCs, $\alpha > 1/3$ are observed for $Ta > 10^8$ and the scaling exponents look $\alpha > 0.38$. It suggests that Cases GTCs are in the ultimate turbulent regime at $Ta > 10^8$ and the transition to the ultimate turbulent regime takes place in $10^7 < Ta < 10^8$. In Case TC, at $Ta > 10^7$, the scaling exponent is $\alpha < 1/3$ and the flow is in the classical tubulent regime. At $Ta \simeq 5\times10^8$, the scaling exponent slightly increases and it suggests that the transition from the classical turbulent regime to the ultimate turbulent regime has started.

Fig.2 (b) shows the mean Nusselt number Nu against Ta, where $Nu = Q_i d/[(T_o - T_i)\lambda\pi r_i L_z]$, Q_i is the heat transfer rate over the inner cylinder and λ is the thermal conductivity. At $Ta \le 10^7$, the scaling exponents of $Nu \sim Ta^\alpha$ are almost the same as $\alpha = 0.25$ irrespective of the presence of the grooves implying that the effects of the grooves on the heat transfer rate is small. At $Ta > 10^7$, the scaling exponent for case TC becomes small to $\alpha = 0.22$ and then goes up to $\alpha = 0.32$, which is similar to the trend of G^ω. These values of α are consistent with the result of Fénot *et al.* (2011) who summarized that the scaling exponent in $Nu \propto Ta^\alpha$ was $\alpha = 0.25 - 0.33$ in non-grooved TC flows. For the grooved cases, the scaling exponent for cases I32 and O48 increases to $\alpha = 0.33$ at $Ta \ge 10^8$, which is also similar to the trend of G^ω.

Contribution of stress components

To evaluate the effect of stresses on G^ω and Nu, their decomposition is applied (Fukagata *et al.*, 2002). Velocity fluctuations are defined as $u' = u - \overline{u}$, where u is the instantaneous velocity and $\overline{u}$ is the time-averaged velocity and $\tilde{u} = u - <u>_{z\theta}$, where $<u>_{z\theta}$ is the velocity averaged in the axial and azimuthal directions. The dimensionless torque G^ω in the present TC flow can be decomposed as

$$G^\omega = 1 + \frac{Re_\tau}{[(r_o - r_i)\omega_i]^+}\int_{r_i}^{r_o}\frac{1}{r}(<\overline{u_r'u_\theta'}>^+_{z\theta} + <\tilde{\overline{u}}_r\tilde{\overline{u}}_\theta>^+_{z\theta})dr + \gamma_v, \qquad (1)$$

where $Re_\tau = u_{\tau,i}d/\nu$ and a value with the superscript + is a value normalized by the inner cylinder friction velocity $u_{\tau,i}$. The first term corresponds to the torque of non-grooved laminar TC flow, the second term is the contribution from the Reynolds stress and the third term is the contribution from the dispersion stress due to the Taylor vortices. The last correction term γ_v appears in the cases of the grooved TC flows and can be written as follows:

$$\gamma_v = \frac{1}{\omega_i}\left[<\frac{\overline{u_\theta}}{r}>_{z\theta}\Big|_{r=r_i} - <\frac{\overline{u_\theta}}{r}>_{z\theta}\Big|_{r=r_o} - \omega_i\right]. \qquad (2)$$

Fig.4 shows the contribution of each term in equation (1) to G^ω. The magnitude of γ_v is marginal for all grooved cases. Up to $Ta \simeq 10^7$, there is no significant difference between the cases while at $Ta \simeq 10^6$, the contribution from the Reynolds stress is dominant. For $Ta > 10^8$, the contribution from the Reynolds stress in Cases GTCs becomes much greater than that of Case TC. Therefore, it can be considered that the development of turbulence reflects the difference of the scaling exponent of G^ω.

For heat transfer, the mean Nusselt number Nu can be decomposed as

$$Nu = \frac{2(1-\eta)}{\ln(1/\eta)\eta} + \frac{2Re_\tau Pr}{r_i\ln(1/\eta)\Delta T^+}\int_{r_i}^{r_o}(<\overline{u_r'T'}>^+_{z\theta} + <\tilde{\overline{u}}_r\tilde{\overline{T}}>^+_{z\theta})dr + \gamma_h, \qquad (3)$$

where $\Delta T = T_o - T_i$. The first term corresponds to the the mean Nusselt number of non-grooved laminar TC flow, the second term is the contribution from the turbulent heat flux and the third term is the contribution from the dispersion heat flux due to the Taylor vortices. The last correction term γ_h appears in the cases of the grooved TC flows and can be written as follows:

$$\gamma_h = \frac{2(1-\eta)}{\Delta T \ln(1/\eta)\eta} \left[< \overline{T} >_{z\theta}\big|_{r=r_o} - < \overline{T} >_{z\theta}\big|_{r=r_i} - \Delta T \right]. \tag{4}$$

Fig.5 shows the contribution of each term in equation (3) to Nu. The effect of γ_h is marginal for all grooved cases. Up to $Ta \simeq 10^7$, there is no significant difference between the cases. For $Ta > 10^8$, the contribution from the turbulent heat flux in Cases GTCs becomes much greater than that of Case TC. This trend is the same as that of G^{ω}.

The effect of grooves

Fig.6 (a) shows the contributions of the pressure drag G_p^{ω} by the grooves to G^{ω}. The contribution by the pressure drag increases with Ta. The same trend is seen in both Cases I32 and O48. Although the rate of the pressure drag is different between the cases. It is approximately 50% of the total torque at $Ta \simeq 5 \times 10^8$ in Case I32 and approximately 80% in Case O48. It is considered that the shape of the groove, especially its depth makes this difference as well as the groove number.

For heat transfer, the heat flux ratio q_r^g/q_r is considered where q_r is the mean radial heat flux over the grooved cylinder surface and q_r^g is its part from the grooves. Fig.6 (b) indicates the contributions from the grooves. In both Cases I32 and O48, the contribution by the grooved part increases with Ta but the change is not significant in Case I32. In Case I32, the non-grooved part is still dominant even at $Ta \simeq 5 \times 10^8$ and occupies approximately 70% of the total heat flux. Compared with Fig.6 (a), it can be seen that the effect of grooves for heat transfer is smaller than that of torque.

Flow structures

To confirm the difference in the flow field transition to the ultimate turbulent regime, the velocity fluctuation in the azimuthal direction u''_{θ} at $(r-r_i)^+ \simeq 10$ from the inner cylinder for the present cases at $Ta \simeq 10^7, 10^8$ is shown in Fig.7. The fluctuation velocity u''_{θ} is defined as $u'' = u - < \overline{u} >_{z\theta}$ where $< \cdot >_{z\theta}$ means the azimuthally and axially averaging. At $Ta \simeq 10^7$, positive $u''_{\theta}/u_{\tau,i}$ corresponds to the outflow region where the high velocity fluids are carried towards the outer cylinder by the Taylor vortices, and turbulent boundary layer (TBL) type streaks are not clearly observed in all cases. At $Ta \simeq 10^8$, Case O48 shows that the streak-like structure extends over the entire axial domain. Ostilla-Mónico *et al.* (2014*b*) reported that the transition to the ultimate regime was caused by turbulence in the boundary layer, and such a flow field is observed in Case O48 at $Ta \simeq 10^8$. In Cases TC and I32 the streaks look limited around the outflow region. This suggests that at $Ta \simeq 10^8$, the transition to the ultimate turbulent regime in Case I32 is not completed.

To see the scales of turbulence, Fig.8 shows the premultiplied energy spectra (PMS) of u''_{θ} near the inner cylinder at $Ta \simeq 10^7$ and 10^8. The λ_z^+ is the normalized wavelength λ_z in the axial direction by the inner cylinder friction velocity $u_{\tau,i}$. In all cases at $Ta \simeq 10^7$, the peak is observed at $\lambda_z/d = 2.5$, which is the wavelength of the Taylor vortices. It shows that the large-scale motions by the Taylor vortex are dominant at this range of Ta. At $Ta \simeq 10^8$, it can be seen that a peak appears around $\lambda_z^+ \simeq 100$ and it coincides the spanwise streak spacing in the turbulent boundary layer. In Case O48, The maximum peak shifts to $\lambda_z^+ \simeq 100$. This suggests that the TBL-like small-scale motions are dominant and they make the transition to the ultimate regime.

CONCLUDING REMARKS

By the DNS and LES for the grooved TC flows with a stationary outer cylinder at the Reynolds number up to $Re = 21000$, the following remarks are obtained.

· For $Ta \leq 10^7$, the scaling exponent α in $G^{\omega} \sim Ta^{\alpha}$ has the same trend regardless the existence of the grooves. For $Ta \geq 10^8$, the effect of the grooves become evident and the torque profile deviates upward from that of Case TC. As for heat transfer, the dependence of Ta on the transition of the scaling exponents in $Nu \sim Ta^{\alpha}$ has similar trend to G^{ω}

· In Case I32, at $Ta \simeq 10^8$ turbulence is not fully developed, while in Case O48, the flow is in the ultimate turbulent regime and the transition to the ultimate turbulent regime takes place in $10^7 < Ta < 10^8$. In Case TC, the flow at $Ta \simeq 10^8$ is still in the classical turbulent regime and the transition from the classical turbulent regime to the ultimate turbulent regime is nearly started.

· The contributions of stress components to G^{ω} are not significantly different at $Ta \leq 10^7$, while at $Ta \geq 10^8$, the contribution from the Reynolds stress becomes dominant for Cases GTCs and it reflects the difference of the scaling exponents of $G^{\omega} \sim Ta^{\alpha}$.

· In regard to the effect of grooves for torque, the pressure drag becomes dominant as Ta increases. For heat transfer, the contribution of the grooved part increases wtih Ta while the effect of grooves is smaller than that of torque.

· At $Ta \simeq 10^7$, the flow structures are similar in all cases and the Taylor vortex motions dominate. At $Ta \simeq 10^8$, streak structures appear in all cases and in Case O48, the maximum peak point of the spectra shifts to $\lambda_z^+ \simeq 100$. This fact suggests that the TBL-type small-scale motions are dominant and they make the transition to the ultimate turbulent regime.

ACKNOWLEDGEMENTS

This work was supported by TRAMI (Transmission Research Association for Mobility Innovation) Grant of 2023 and JHPCN projects jh230007 and jh240042.

REFERENCES

Bouafia, M., Bartin, Y., Saulnier, J.B. & Ropert, P. 1998 *Int. J. Heat Mass Transfer* **41** (10), 1279–1291.

Fénot, M., Bertin, Y., Dorignac, E. & Lalizel, G. 2011 *Int. J Therm. Sci.* **50** (7), 1138–1155.

Fukagata, K., Iwamoto, K. & Kasagi, N. 2002 *Physics of fluids* **14** (11), L73–L76.

Grossmann, S., Lohse, D. & Sun, C. 2016 *Annu. Rev. Fluid Mech.* **48**, 53–80.

Lévêque, E., Toschi, F., Shao, L. & Bertoglio, J. P. 2007 *J. Fluid Mech* **570**, 491–502.

Ostilla-Mónico, R., Huisman, S. G., Jannink, T. J. G., Van Gils, D. P. M., Verzicco, R., Grossmann, S., Sun, C. & Lohse, D. 2014*a J. Fluid Mech.* **747**, 1–29.

Ostilla-Mónico, R, Van Der Poel, E. P., Verzicco, R, Grossmann, S & Lohse, D 2014*b Physics of Fluids* **26** (1).

Suga, K., Chikasue, R. & Kuwata, Y. 2017 Modelling turbulent and dispersion heat fluxes in turbulent porous medium flows using the resolved les data. *Int. J. Heat and Fluid Flow* **68**, 225–236.

Suga, K., Kuwata, Y., Takashima, K. & Chikasue, R. 2015 *Comput. Math. Appl.* **69** (6), 518–529.

Zhu, X., Verschoof, R. A., Bakhuis, D., Huisman, S. G., Verzicco, R., Sun, C. & Lohse, D. 2018 *Nature phys.* **14** (4), 417–423.

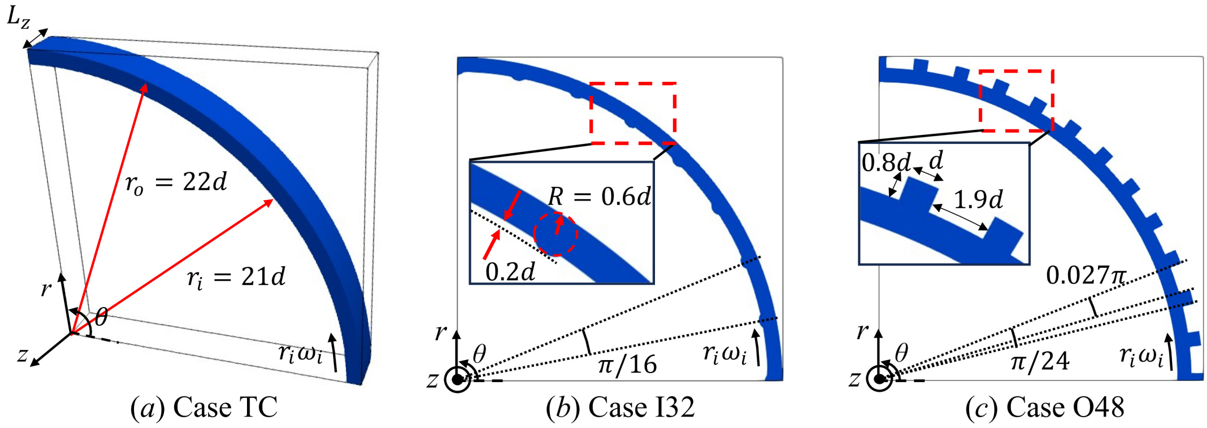

Figure 1. Computational domains and geometries for TC flows (a), grooved TC flows of Case I32 (b) and Case O48 (c).

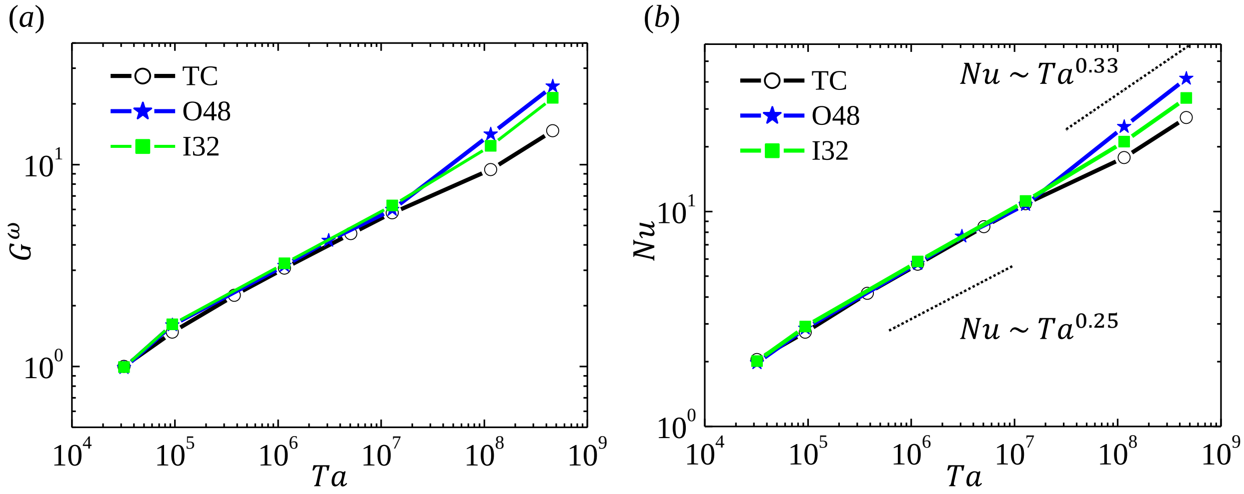

Figure 2. Torque and heat transfer as functions of Ta: (a) dimensionless torque G^ω, (b) mean Nusselt number Nu.

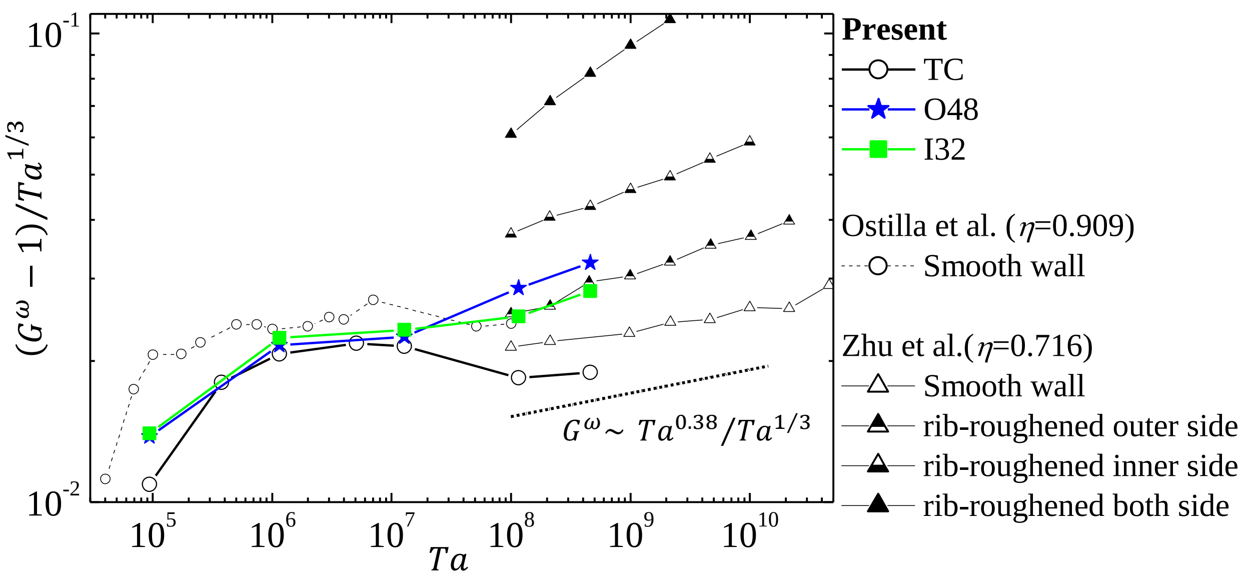

Figure 3. Compenseted dimensionless torque as function of Ta. The reference data are from Ostilla-Mónico *et al.* (2014a) and Zhu *et al.* (2018).

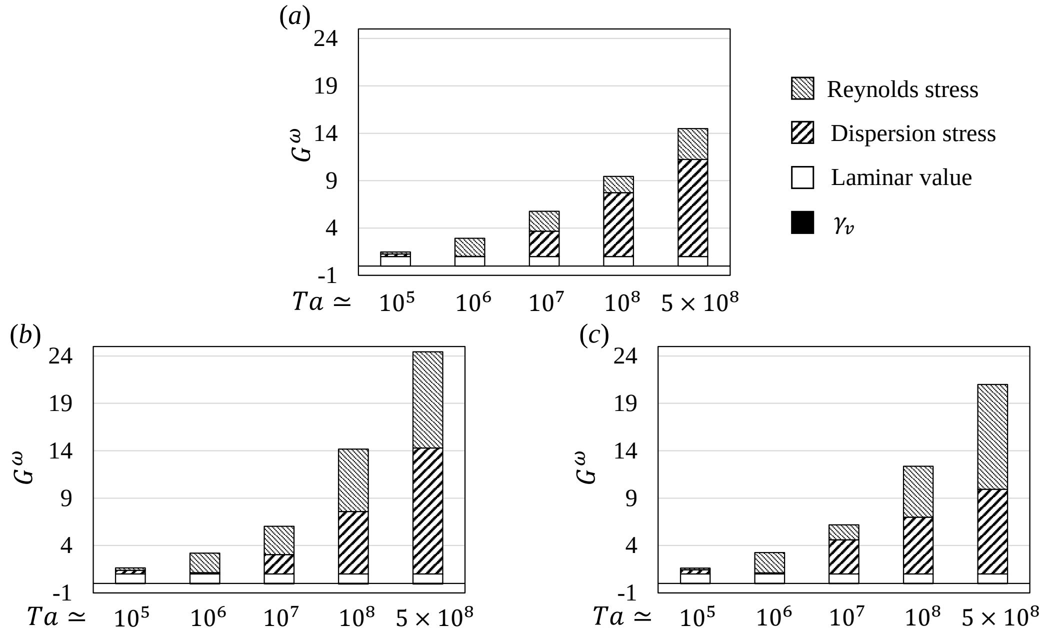

Figure 4. Contribution of each term to the dimensionless torque: (*a*) Case TC, (*b*) Case O48, (*c*) Case I32.

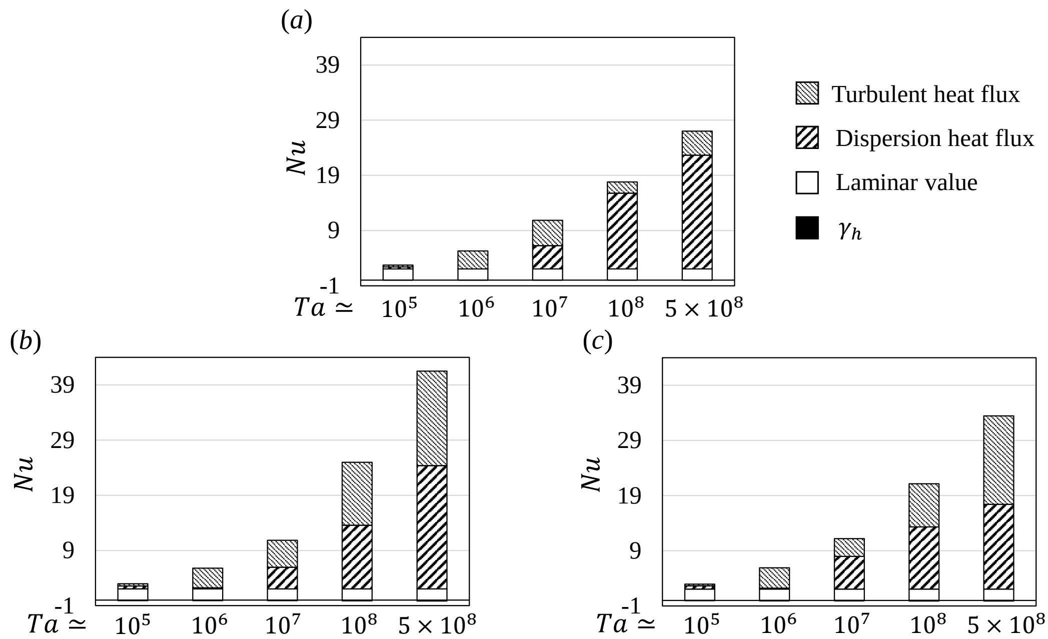

Figure 5. Contribution of each term to the mean Nusselt number: (*a*) Case TC, (*b*) Case O48, (*c*) Case I32.

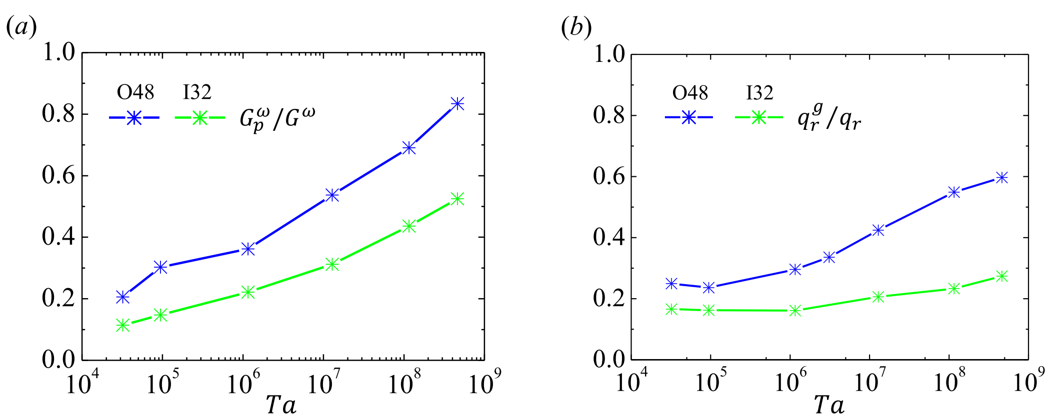

Figure 6. Effects of grooves on torque and heat transfer: (*a*) torque ratio of the pressure drag, (*b*) heat flux ratio of the grooved parts.

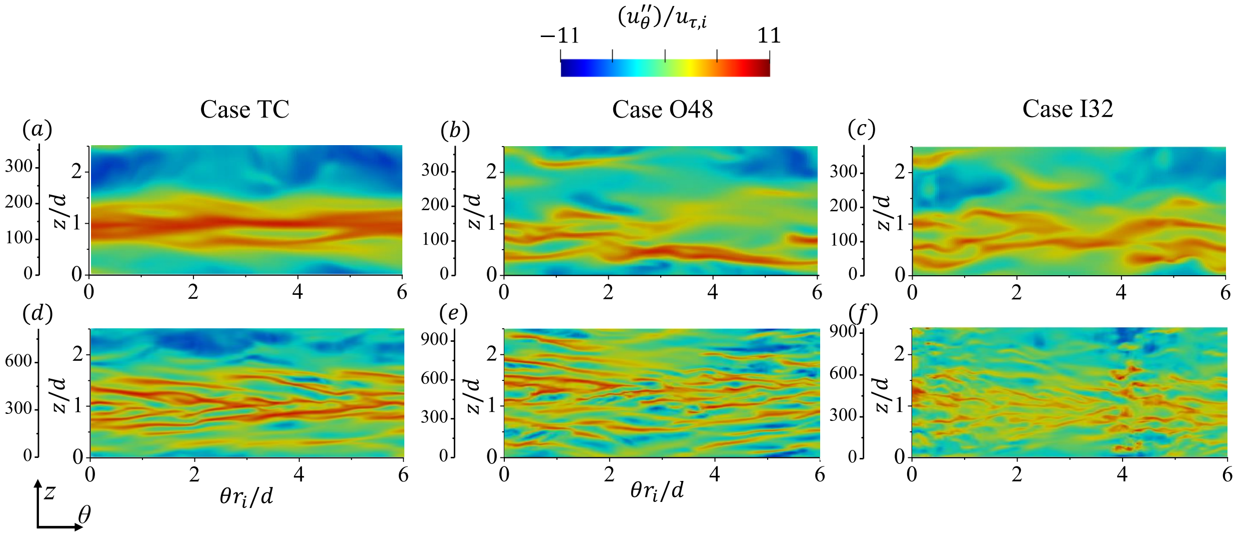

Figure 7. Instantaneous azimuthal velocity fluctuation u''_θ in the axial-azimuthal plane: (*a*, *d*) Case TC, (*b*, *e*) Case O48 and (*c*, *f*) Case I32 at (*a*, *b*, *c*) $Ta \simeq 10^7$ and (*d*, *e*, *f*) $Ta \simeq 10^8$.

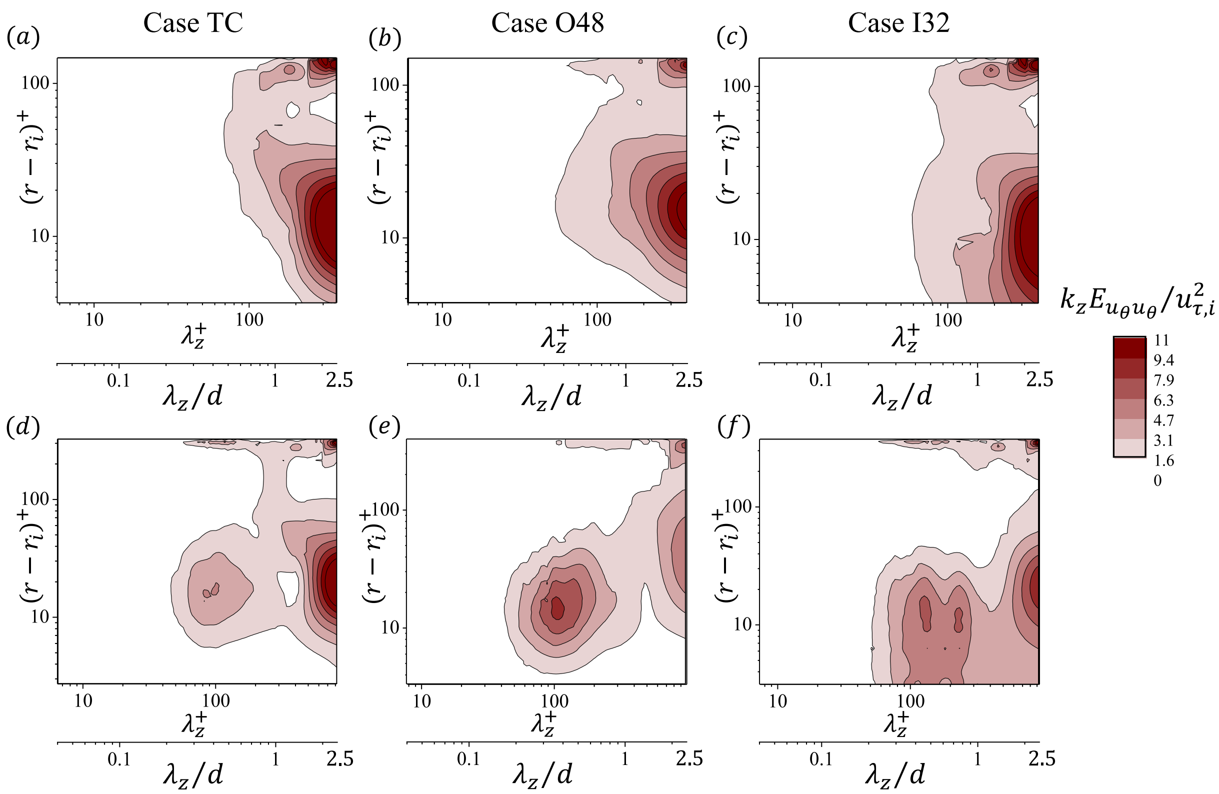

Figure 8. The pre-multiplied spanwise energy spectra of u''_θ: (*a*, *d*) Case TC , (*b*, *e*) Case O48 and (*c*, *f*) Case I32 at (*a*, *b*, *c*) $Ta \simeq 10^7$ and (*d*, *e*, *f*) $Ta \simeq 10^8$.